

**Millimeter-wave spectroscopy of CrC ( $X^3\Sigma^-$ ) and CrCCH ( $\tilde{X}^6\Sigma^+$ ): Examining the chromium-carbon bond**

J. Min and L. M. Ziurys

Citation: *The Journal of Chemical Physics* **144**, 184308 (2016); doi: 10.1063/1.4947247

View online: <http://dx.doi.org/10.1063/1.4947247>

View Table of Contents: <http://scitation.aip.org/content/aip/journal/jcp/144/18?ver=pdfcov>

Published by the **AIP Publishing**

---

**Articles you may be interested in**

[Millimeter-wave spectroscopy of the FeCO radical in the  \$v\_2\$  and  \$v\_3\$  vibrationally excited states](#)

*J. Chem. Phys.* **143**, 014303 (2015); 10.1063/1.4923215

[Millimeter-wave rotational spectroscopy of FeCN \( \$X^4\Delta\_i\$ \) and FeNC \( \$X^6\Delta\_i\$ \): Determining the lowest energy isomer](#)

*J. Chem. Phys.* **135**, 184303 (2011); 10.1063/1.3653809

[The rotational spectrum of CuCCH \( \$X^1\Sigma^+\$ \): A Fourier transform microwave discharge assisted laser ablation spectroscopy and millimeter/submillimeter study](#)

*J. Chem. Phys.* **133**, 174301 (2010); 10.1063/1.3493690

[Molecules in high spin states III: The millimeter/submillimeter-wave spectrum of the MnCl radical \( \$X^7\Sigma^+\$ \)](#)

*J. Chem. Phys.* **122**, 054309 (2005); 10.1063/1.1824036

[Gas phase spectroscopy of alkali carbides: The pure rotational spectrum of KC \( \$X^4\Sigma^-\$ \)](#)

*J. Chem. Phys.* **110**, 4797 (1999); 10.1063/1.478367

---



**NEW Special Topic Sections**

**NOW ONLINE**  
Lithium Niobate Properties and Applications:  
Reviews of Emerging Trends

**AIP** | Applied Physics  
Reviews

# Millimeter-wave spectroscopy of CrC ( $X^3\Sigma^-$ ) and CrCCH ( $\tilde{X}^6\Sigma^+$ ): Examining the chromium-carbon bond

J. Min and L. M. Ziurys<sup>a)</sup>

Department of Chemistry and Biochemistry, Department of Astronomy, Steward Observatory,  
 933 North Cherry Avenue, University of Arizona, Tucson, Arizona 85721, USA

(Received 27 January 2016; accepted 9 April 2016; published online 13 May 2016)

Pure rotational spectroscopy of the CrC ( $X^3\Sigma^-$ ) and CrCCH ( $\tilde{X}^6\Sigma^+$ ) radicals has been conducted using millimeter/sub-millimeter direct absorption methods in the frequency range 225–585 GHz. These species were created in an AC discharge of Cr(CO)<sub>6</sub> and either methane or acetylene, diluted in argon. Spectra of the CrCCD were also recorded for the first time using deuterated acetylene as the carbon precursor. Seven rotational transitions of CrC were measured, each consisting of three widely spaced, fine structure components, arising from spin-spin and spin-rotation interactions. Eleven rotational transitions were recorded for CrCCH and five for CrCCD; each transition in these cases was composed of a distinct fine structure sextet. These measurements confirm the respective  $^3\Sigma^-$  and  $^6\Sigma^+$  ground electronic states of these radicals, as indicated from optical studies. The data were analyzed using a Hund's case (b) Hamiltonian, and rotational, spin-spin, and spin-rotation constants have been accurately determined for all three species. The spectroscopic parameters for CrC were significantly revised from previous optical work, while those for CrCCH are in excellent agreement; completely new constants were established for CrCCD. The chromium-carbon bond length for CrC was calculated to be 1.631 Å, while that in CrCCH was found to be  $r_{\text{Cr-C}} = 1.993$  Å — significantly longer. This result suggests that a single Cr—C bond is present in CrCCH, preserving the acetylenic structure of the ligand, while a triple bond exists in CrC. Analysis of the spin constants suggests that CrC has a nearby excited  $^1\Sigma^+$  state lying  $\sim 16900$  cm<sup>-1</sup> higher in energy, and CrCCH has a  $^6\Pi$  excited state with  $E \sim 4800$  cm<sup>-1</sup>. *Published by AIP Publishing.* [<http://dx.doi.org/10.1063/1.4947247>]

## I. INTRODUCTION

Chromium plays a versatile role in organometallic synthesis, mainly because of its wide range of available oxidation states from -IV to +VI.<sup>1</sup> The element has many applications, such as in the development of stereoselective (arene) reagents, more efficient polymerization catalysts, and novel molecules with unusual oxidation. A common appearance of chromium is in carbonyl complexes and cyclopentadienyl sandwich compounds,<sup>2</sup> such as chromocene. Recently, calculations have suggested that dimetallocenes with chromium may be useful for H<sub>2</sub> storage.<sup>3</sup>

Chromium also plays a role in carbon clusters. Early transition metals such as chromium have been found to form stable gas-phase metal-carbon clusters, metalcarbohedrenes, or “metcars,” with the general formula M<sub>8</sub>C<sub>12</sub><sup>+</sup>.<sup>4</sup> Chromium, however, does not appear to form either endohedral or exohedral metallofullerenes, as do other transition metals (e.g., Refs. 5 and 6). Titanium, for example, figures prominently in metcars but also can be incorporated inside fullerenes, such as in Ti<sub>2</sub>C<sub>2</sub>@C<sub>78</sub>, and can be attached to the outside of C<sub>60</sub>.<sup>7</sup> The apparent lack of chromium complexes with fullerenes may arise from a weak Cr—C<sub>2</sub> bond, as predicted by theory.<sup>8</sup> This

bond principally occurs between the sd<sub>σ</sub> hybridized orbital on the metal atom and the unoccupied 3σ<sub>g</sub> orbital of the C<sub>2</sub> moiety. However, more experimental data are needed to probe the chromium-carbon bond.

High-resolution gas-phase spectroscopy of small model systems provides an important avenue to examine metal-carbon bonding. In the case of 3d transition metals, species of the type MC, MCCH, MCH, MCH<sub>3</sub>, and MC<sub>2</sub> have been studied to date. For the dicarbide compounds, only ScC<sub>2</sub> thus far has been investigated, in this instance by Fourier transform microwave/mm-wave methods.<sup>9</sup> This work showed that the molecule has a T-shaped geometry, as suggested by theory.<sup>8</sup> In the case of the diatomic carbides, optical spectroscopy has been carried out for FeC, CoC, NiC, VC, and, more recently, TiC.<sup>10–14</sup> Pure rotational data have been recorded for FeC, CoC, and NiC as well.<sup>15,16</sup> These studies have demonstrated that the ground states of these molecules are  $^3\Delta$ ,  $^2\Sigma^+$ ,  $^1\Sigma^+$ ,  $^2\Delta$ , and  $^3\Sigma^+$ , respectively. For the metal monoacetylides, CuCCH and ZnCCH have been characterized using pure rotational spectroscopy,<sup>17,18</sup> and recently NiCCH and CuCCH have been studied in the optical regime.<sup>19,20</sup> Besides identifying electronic states, such work suggested that the CCH moiety retains an acetylenic structure when bonded to copper or zinc. VCH and TiCH have also been studied in the optical regime by Merer and collaborators, who found their structures to be linear.<sup>21,22</sup> The pure rotational spectrum

<sup>a)</sup> Author to whom correspondence should be addressed. Electronic mail: lziurys@email.arizona.edu. Fax: 520-621-1532.

of  $\text{CuCH}_3$  has additionally been measured, revealing its  $C_{3v}$  symmetry.<sup>23</sup> Vibrationally resolved spectra of  $\text{NiCH}_3$  has also been recorded.<sup>24</sup>

Spectroscopic studies of chromium-bearing molecules have been almost exclusively the work of Morse and collaborators. These authors have recorded vibrationally resolved spectra of the  ${}^6\tilde{E}-\tilde{X}{}^6A_1$  transition of  $\text{CrCH}_3$  and the  $\tilde{A}{}^6\Sigma^+-\tilde{X}{}^6\Sigma^+$  system of  $\text{CrCCH}$ <sup>24</sup> using resonant two-photon ionization (R2PI) methods; they also measured the  ${}^3\Sigma^--X{}^3\Sigma^-$  system of  $\text{CrC}$  with rotational resolution.<sup>25</sup> A very recent work has produced a detailed rotational analysis of the  $3^1_0$  band of the  $\tilde{A}-\tilde{X}$  transition of  $\text{CrCCH}$ .<sup>26</sup> These chromium species were all produced by laser ablation of the metal in a dilute mixture of methane in helium.

Here we present the first measurements of pure rotational spectra of  $\text{CrC}$  and  $\text{CrCCH}$  in their respective  $X{}^3\Sigma^-$  and  $\tilde{X}{}^6\Sigma^+$  ground electronic states. In order to confirm the identification of the monoacetylide, transitions were also recorded for  $\text{CrCCD}$ —the first observation of this species. These molecules were investigated using millimeter-wave direct absorption methods with organometallic precursors, allowing accurate determination of their spectroscopic constants. From these parameters, Cr—C bond lengths have been calculated, as well as estimates of the energies of nearby excited states. In this paper, we present our data and their respective spectral analyses and provide insight into the bonding in chromium-bearing molecules.

## II. EXPERIMENT

The measurements for  $\text{CrC}$  ( $X{}^3\Sigma^-$ ) and  $\text{CrCCH}$  ( $\tilde{X}{}^6\Sigma^+$ ) were conducted with one of the direct absorption spectrometers of the Ziurys group, which has been described in detail elsewhere.<sup>27,28</sup> Briefly, the radiation source for this instrument consists of phase-locked Gunn oscillators that are used in conjunction with various Schottky diode multipliers, providing nearly continuous frequency coverage across the range 65–850 GHz. The reaction chamber is a methanol-chilled, 85 cm-long single-pass glass cell containing two ring electrodes at either ends which support a longitudinal AC discharge. The detector is a helium-cooled hot electron bolometer. The radiation is propagated quasi-optically through the cell by a series of Teflon lenses. Phase-sensitive detection is achieved by FM modulation of the Gunn oscillator through the phase-lock loop.

The molecules were created in an AC discharge of  $\text{Cr}(\text{CO})_6$ , argon, and either methane ( $\text{CrC}$ ) or acetylene ( $\text{CrCCH}$ ). For  $\text{CrCCD}$ , deuterated acetylene was used as the precursor. Solid  $\text{Cr}(\text{CO})_6$  was placed in a small metal tube attached to the cell and heated to about 85 °F, creating ~1 mTorr of vapor. Approximately 1 mTorr of methane and 50 mTorr of argon maximized the signals for  $\text{CrC}$ , while the optimal mixture for  $\text{CrCCH}$  was ~0.5 mTorr of acetylene and 40 mTorr of argon. The AC discharge was modulated at a rate of 20 kHz with 250 W of power for all syntheses.

Transition frequencies were measured by averaging 4–10 scans, half taken in increasing frequency and the rest in decreasing frequency, each 5 MHz in width. The recorded line shapes were fit with Gaussian profiles to establish the

center frequencies. Line widths ranged from 0.4 to 1.5 MHz over the range 225–580 GHz. Given the signal-to-noise ratios for the recorded lines, measurement of the  ${}^{53}\text{Cr}$  isotopologues was not attempted. This isotope of chromium is roughly 1/9th of the abundance of  ${}^{52}\text{Cr}$ ; it also has a nuclear spin, and thus additional splittings would further reduce the strength of observed features.

## III. RESULTS

The initial search for  $\text{CrC}$  ( $X{}^3\Sigma^-$ ) was guided by the rotational constant of ~19.8 GHz determined by the optical work.<sup>25</sup> Initially a range of about 100 GHz, or  $5B$ , was continuously scanned to prevent misassignments, for example, if an excited state was present. Only rarely have excited electronic states been observed in such rotational data, and only when the ground state signals were extremely intense—not the case in these studies. For a  ${}^3\Sigma^-$  term, each rotational level  $N$  is split into three fine structure sub-levels with  $J = N - 1$ ,  $N$ , and  $N + 1$ , where  $J = N + S$ , as shown in the qualitative energy level diagram presented in Figure 1. The splitting arises from a combination of spin-rotation ( $N \cdot S$ ) and spin-spin ( $S \cdot S$ ) interactions. The most favored transitions occur for  $\Delta N = \Delta J = +1$  (for absorption), as shown in the figure. Therefore, every rotational transition consists of three strong fine structure components, which appear as a nominal triplet in the case (b) limit, where  $B \sim \lambda$  and  $\lambda$  is the spin-spin constant. Only transitions from the  $J = N$  component follow a harmonic pattern—the starting point for the search. Five successive harmonically-related lines corresponding to a rotational constant near 19 GHz were found in the data; these features disappeared upon removal of  $\text{Cr}(\text{CO})_6$ , suggesting that they arose from a chromium-containing species. The other two spin components for  $\text{CrC}$  were then identified after considerable searching, revealing a “classic” case (b) triplet.

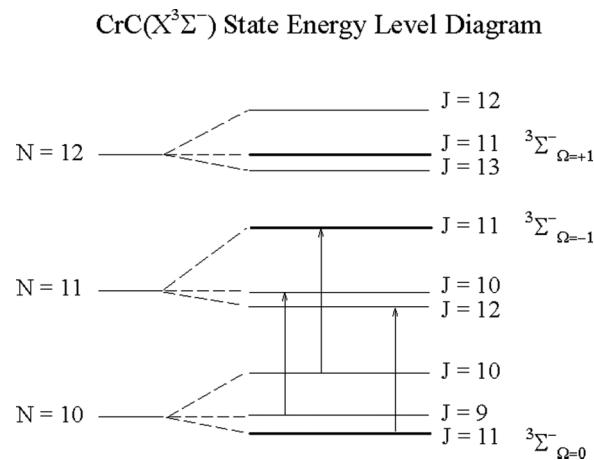


FIG. 1. Qualitative energy level diagram of  $\text{CrC}$  ( $X{}^3\Sigma^-$ ), showing the fine structure splittings and favorable transitions, indicated by arrows, which generate the characteristic triplet pattern in this free radical. Also portrayed is the shifting of energy levels by interaction with the isoconfigurational  ${}^1\Sigma^+$  excited state through second-order spin-orbit coupling. For a given  $J$  (in this case  $J = 11$ , shown in bold), the  $\Omega = 0$  sub-level ( ${}^3\Sigma^-_{\Omega=0}$ ) moves to lower energy relative to the  $\Omega = 1$  sub-levels ( ${}^3\Sigma^-_{\Omega=\pm 1}$ ); see text.

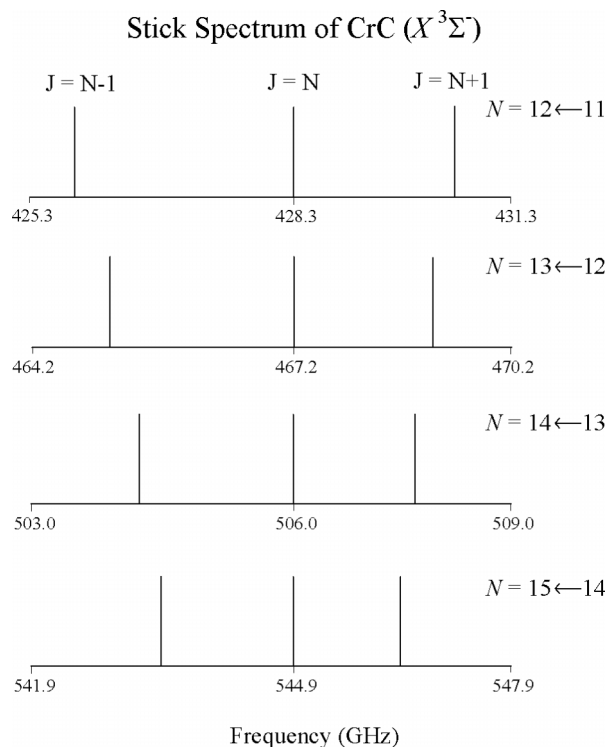


FIG. 2. Stick diagram of the  $N = 12 \leftarrow 11$ ,  $13 \leftarrow 12$ ,  $14 \leftarrow 13$ , and  $15 \leftarrow 14$  rotational transitions of  $\text{CrC} (X^3\Sigma^-)$ , near 428, 467, 506, and 545 GHz, respectively, illustrating the variation in the triplet spin pattern as a function of  $N$ . The separation of the three fine structure components decreases with increasing frequency. Recognition of this pattern is key to the identification of  $\text{CrC}$ .

Figure 2 illustrates the triplet structure of  $\text{CrC}$ , displayed as stick spectra for four consecutive rotational transitions. For the  $N = 15 \leftarrow 14$  transition (lowest spectrum), the pattern is fairly symmetric, with the  $J = N + 1$  and  $N - 1$  lines located  $\sim 1.2$  and  $1.4$  GHz from the center,  $J = N$  component. As  $N$  decreases, the splitting becomes more asymmetric, increasing to  $1.7$  and  $2.3$  GHz from the center feature for the  $N = 12 \leftarrow 11$  transition (top spectrum).

In Figure 3, typical spectra measured for  $\text{CrC}$  are presented. The fine structure triplet of the  $N = 12 \leftarrow 11$ ,  $13 \leftarrow 12$ , and  $14 \leftarrow 13$  rotational transitions near 467, 506, and 545 GHz are displayed. There are two frequency breaks in each spectrum to show all three fine structure lines, labeled by quantum number  $J$ . The actual splitting is more asymmetric, as Figure 2 shows.

The transition frequencies recorded for the  $\text{CrC}$  radical are presented in Table I. Seven rotational transitions  $N + 1 \leftarrow N$ , each consisting of three fine-structure components, were measured—total of 21 individual lines.

In the case of  $\text{CrCCH}$ , the frequency range 450–480 GHz was continuously scanned, based on a rotational constant of  $B = 3843$  MHz provided by the optical studies.<sup>24,26</sup> The ground state of  $\text{CrCCH}$  is  $^6\Sigma^+$ . As illustrated in Figure 4, each rotational level for this term, indicated by  $N$ , is split into six fine structure components, labeled by  $J$ . The splittings arise from spin-spin coupling, described by the constant  $\lambda$ , and the spin-rotation interactions, characterized by  $\gamma$ . Again, the strongest transitions  $N + 1 \leftarrow N$  occur for  $\Delta N = \Delta J = +1$ ,

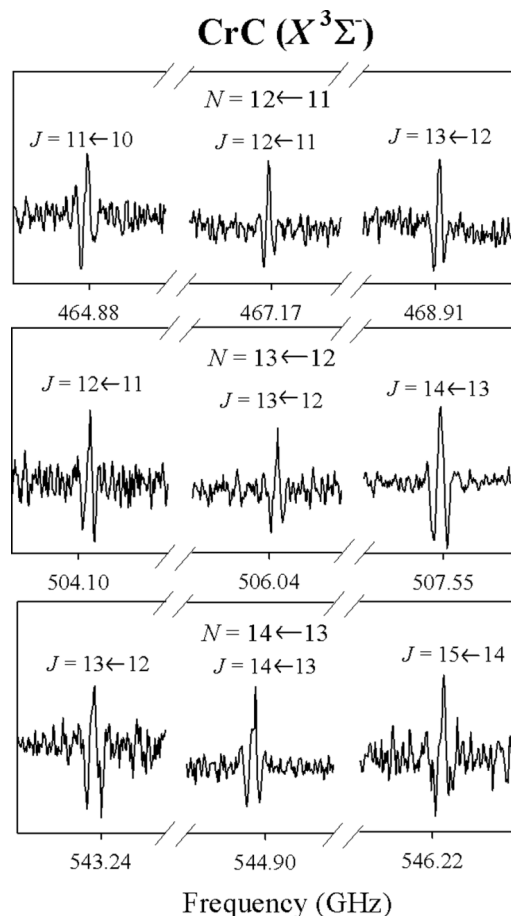


FIG. 3. Millimeter-wave spectra of  $N = 12 \leftarrow 11$ ,  $13 \leftarrow 12$ , and  $14 \leftarrow 13$  rotational transitions of  $\text{CrC} (X^3\Sigma^-)$  measured in this work near 467–545 GHz. Each transition  $N + 1 \leftarrow N$  consists of three fine-structure components, indicated by quantum number  $J$ , which are clearly resolved and form an asymmetric triplet pattern. There are two frequency breaks in the display of each transition to show the three lines. The spectral features exhibit a second derivative profile due to use of phase-sensitive detection at  $2f$ . Each fine-structure component was measured using a 110 MHz-wide scan obtained in 70 s, and then cropped to display  $\sim 50$  MHz.

generating a fine structure sextet. A series of four sextets, one which first appeared to be a quintet, were identified in the data from the broad-band search, and were found to be separated by approximately  $2B$ . These spectral lines disappeared upon removal of either  $\text{Cr}(\text{CO})_6$  or acetylene. The overall sextet fine-structure splitting spanned about 250 MHz, with the individual components separated relatively evenly by about 50 MHz. After the four sextets were identified, other transitions were measured.

A search was also carried out for the deuterated analog,  $\text{CrCCD}$ , to confirm the identification of  $\text{CrCCH}$ . A rotational constant was estimated by scaling that of  $\text{CrCCH}$  by the ratio  $B(\text{ZnCCD})/B(\text{ZnCCH})$  from Ref. 18. Based on this constant, another series of sextets were located with a slightly smaller fine structure splitting ( $\sim 40$  MHz). These features could only be generated in the presence of both  $\text{Cr}(\text{CO})_6$  and  $\text{DCCD}$ , and therefore were identified as arising from  $\text{CrCCD}$ .

A total of eleven rotational transitions of  $\text{CrCCH}$  were recorded in the frequency range 245–483 GHz, each consisting of six fine structure components, as presented in

TABLE I. Observed rotational transitions of CrC ( $X^3\Sigma^-$ ).<sup>a</sup>

$N'$	$J'$	$N''$	$J''$	$\nu_{\text{obs}}$	$\nu_{\text{o-c}}$
6	5	5	4	225 108.933	0.072
6	6	5	5	233 714.325	-0.140
6	7	5	6	238 899.060	0.105
7	6	6	5	266 070.353	-0.039
7	7	6	6	272 648.986	0.007
7	8	6	7	276 798.982	-0.020
11	10	10	9	425 546.213	-0.071
11	11	10	10	428 292.552	-0.079
11	12	10	11	430 303.686	-0.042
12	11	11	10	464 879.555	0.163
12	12	11	11	467 174.084	0.041
12	13	11	12	468 906.736	-0.021
13	12	12	11	504 102.167	0.021
13	13	12	12	506 041.312	0.018
13	14	12	13	507 549.180	0.006
14	13	13	12	543 238.397	-0.039
14	14	13	13	544 893.264	0.059
14	15	13	14	546 217.295	0.056
15	14	14	13	582 304.589	-0.067
15	15	14	14	583 728.603	0.007
15	16	14	15	584 900.587	-0.046

<sup>a</sup>In MHz.

Table II. A total of 66 individual lines were measured. Five rotational transitions were measured for CrCCD in the region 451–487 GHz, also composed of fine structure sextets. These data, a total of 29 individual features, are shown in Table III.

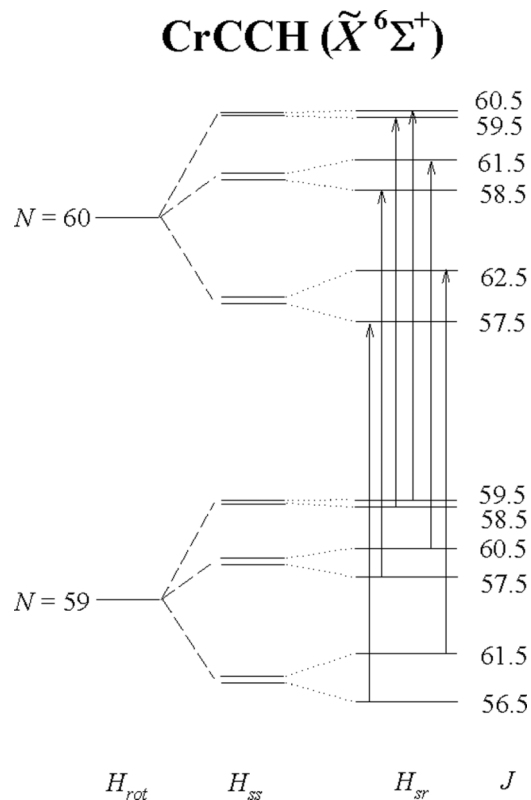


FIG. 4. Qualitative energy level diagram of CrCCH ( $\tilde{X}^6\Sigma^+$ ) showing the  $N = 59$  and  $60$  rotational levels and the fine structure sub-levels generated by spin-spin and spin-rotation interactions. The favorable transitions are shown by arrows and produce a distinctive sextet pattern.

TABLE II. Observed rotational transitions of CrCCH ( $\tilde{X}^6\Sigma^+$ ).<sup>a</sup>

$N'$	$J'$	$N''$	$J''$	$\nu_{\text{obs}}$	$\nu_{\text{o-c}}$
32	29.5	31	28.5	245 858.254	0.011
	30.5		29.5	245 902.139	0.149
	31.5		30.5	245 958.936	-0.061
	32.5		31.5	246 016.752	0.118
	33.5		32.5	246 069.495	-0.067
	34.5		33.5	246 114.605	0.156
33	30.5	32	29.5	253 535.282	-0.151
	31.5		30.5	253 579.406	0.036
	32.5		31.5	253 635.696	-0.057
	33.5		32.5	253 692.850	-0.019
	34.5		33.5	253 745.602	-0.038
	35.5		34.5	253 790.897	0.064
35	32.5	34	31.5	268 886.760	0.045
	33.5		32.5	268 930.976	-0.009
	34.5		33.5	268 986.200	-0.096
	35.5		34.5	269 042.516	0.020
	36.5		35.5	269 094.937	-0.047
	37.5		36.5	269 140.747	0.030
36	33.5	35	32.5	276 560.745	-0.017
	34.5		33.5	276 605.206	0.029
	35.5		34.5	276 660.203	0.177
	36.5		35.5	276 715.818	-0.004
	37.5		36.5	276 768.194	0.012
	38.5		37.5	276 814.207	0.051
37	34.5	36	33.5	284 233.652	-0.062
	35.5		34.5	284 278.181	-0.082
	36.5		35.5	284 332.547	-0.142
	37.5		36.5	284 388.233	0.120
	38.5		37.5	284 440.335	-0.018
	39.5		38.5	284 486.555	0.003
58	55.5	57	54.5	445 065.154	-0.100
	56.5		55.5	445 111.045	0.025
	57.5		56.5	445 161.120	-0.055
	58.5		57.5	445 212.588	-0.038
	59.5		58.5	445 263.454	-0.088
59	60.5	58	59.5	445 312.362	-0.032
	56.5		56.5	452 707.117	-0.101
	57.5		57.5	452 752.999	-0.001
	58.5		58.5	452 803.067	0.009
	59.5		59.5	452 854.452	0.036
	60.5		60.5	452 905.500	0.197
60	61.5	59	60.5	452 954.147	-0.083
	57.5		57.5	460 347.418	-0.028
	58.5		58.5	460 393.232	-0.010
	59.5		59.5	460 443.172	-0.034
	60.5		60.5	460 494.406	-0.070
	61.5		61.5	460 545.284	-0.052
61	62.5	60	61.5	460 594.256	-0.080
	58.5		58.5	467 986.042	0.135
	59.5		59.5	468 031.739	0.024
	60.5		60.5	468 081.566	-0.025
	61.5		61.5	468 132.798	0.021
	62.5		62.5	468 183.505	-0.106
	63.5		63.5	468 232.640	-0.043
62	59.5	61	58.5	475 622.609	0.035
	60.5		59.5	475 668.407	0.015
	61.5		60.5	475 718.238	0.056
	62.5		61.5	475 769.296	0.007
	63.5		62.5	475 820.025	-0.074
	64.5		63.5	475 869.193	-0.046

TABLE II. (Continued.)

$N'$	$J'$	$N''$	$J''$	$\nu_{\text{obs}}$	$\nu_{0-c}$
63	60.5	62	59.5	483 257.551	0.135
	61.5		60.5	483 303.304	0.061
	62.5		61.5	483 353.007	0.055
	63.5		62.5	483 404.077	0.095
	64.5		63.5	483 454.650	-0.120
	65.5		64.5	483 504.150	0.173

<sup>a</sup>In MHz.

(One component could not be measured in the  $N = 67 \leftarrow 66$  transitions because of a contaminating line.)

Representative spectra of CrCCH are shown in Figure 5. Here the  $N = 60 \leftarrow 59$ ,  $61 \leftarrow 60$ , and  $62 \leftarrow 61$  rotational transitions near 460–475 GHz are presented. The fine structure sextets, labeled by quantum number  $J$  and separated by  $\sim 50$  MHz, are clearly evident in each spectrum—solid evidence for the  ${}^6\Sigma^+$  ground state. Figure 6 shows the spectrum of the  $N = 64 \leftarrow 63$  transition of CrCCD near 451 GHz. Again, the sextet pattern, indicated by  $J$ , is plainly visible, but the overall fine structure splitting is slightly smaller than in CrCCH. This difference is expected, as the spin-rotation constant and to some extent the spin-spin constant scale with  $B$ .

TABLE III. Observed rotational transitions of CrCCD ( $\tilde{X} {}^6\Sigma^+$ ).<sup>a</sup>

$N'$	$J'$	$N''$	$J''$	$\nu_{\text{obs}}$	$\nu_{0-c}$
64	61.5	63	60.5	451 605.361	0.010
	62.5		61.5	451 646.763	-0.020
	63.5		62.5	451 693.905	-0.019
	64.5		63.5	451 742.742	0.047
	65.5		64.5	451 790.268	0.018
	66.5		65.5	451 834.606	-0.010
65	62.5	64	61.5	458 630.791	-0.026
	63.5		62.5	458 672.288	0.006
	64.5		63.5	458 719.306	-0.003
	65.5		64.5	458 767.989	0.029
	66.5		65.5	458 815.483	0.008
	67.5		66.5	458 859.934	0.008
66	63.5	65	62.5	465 654.733	-0.023
	64.5		63.5	465 696.309	0.059
	65.5		64.5	465 743.162	-0.006
	66.5		65.5	465 791.493	-0.212
	67.5		66.5	465 839.247	0.065
	68.5		67.5	465 883.727	0.012
67	64.5	66	63.5	472 677.120	-0.023
	65.5		64.5	...	...
	66.5		65.5	472 765.486	0.008
	67.5		66.5	472 813.922	0.016
	68.5		67.5	472 861.420	0.073
	69.5		68.5	472 905.937	-0.023
69	66.5	68	65.5	486 717.206	0.036
	67.5		66.5	486 758.761	0.020
	68.5		67.5	486 805.384	0.027
	69.5		68.5	486 853.544	-0.037
	70.5		69.5	486 900.952	-0.003
	71.5		70.5	486 945.684	-0.037

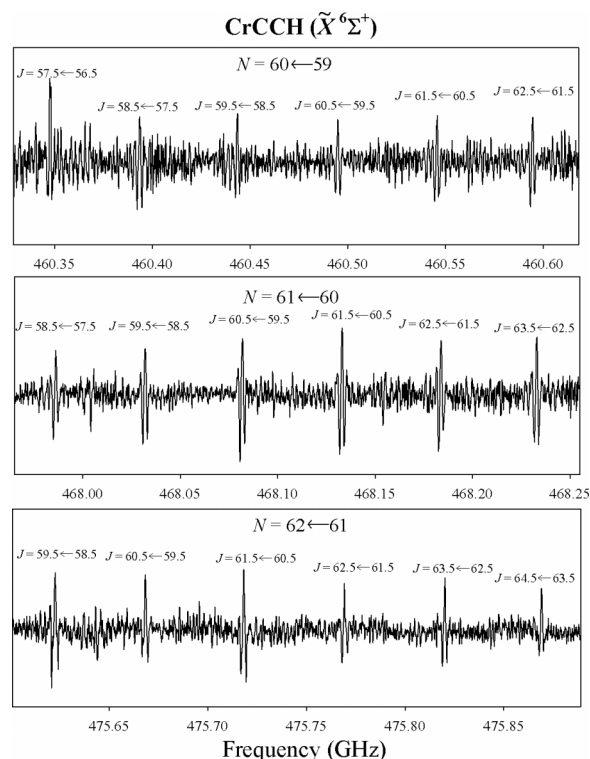
<sup>a</sup>In MHz.

FIG. 5. Millimeter-wave spectra of the  $N = 60 \leftarrow 59$ ,  $61 \leftarrow 60$ , and  $62 \leftarrow 61$  rotational transitions of CrCCH. Each transition  $N + 1 \leftarrow N$  consists of six fine-structure components, labeled by quantum number  $J$ , which compose a rather regular fine-structure sextet, indicating the  ${}^6\Sigma^+$  ground state. The spectral features exhibit a second derivative line profile due to use of phase-sensitive detection at  $2f$ . Each spectrum is a composite of three, 110 MHz wide scans which were individually acquired in 70 s.

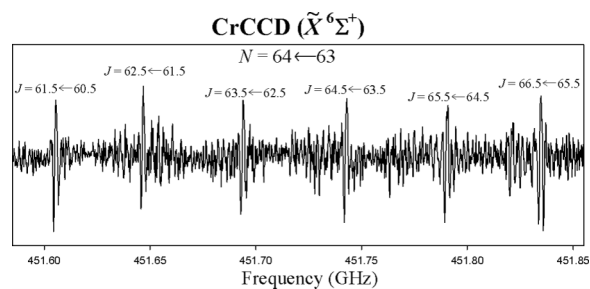


FIG. 6. Millimeter-wave spectrum of the  $N = 64 \leftarrow 63$  transition of CrCCD near 451 GHz. The transition consists of six fine-structure components, indicated by quantum number  $J$ , which compose a fine-structure sextet with somewhat different splittings from the main isotopologue. The spectral features exhibit a second derivative profile due to use of phase-sensitive detection at  $2f$ . The spectrum is a composite of three, 110 MHz-wide scans which were individually acquired in 70 s.

Unassigned lines were also found in the data. Typically, 30%-50% of observed spectral features are not identified. Many likely arise from other radical species containing only carbon and hydrogen. Chromium-bearing radicals such as  $\text{CrCH}_2$  are also possibilities.

#### IV. ANALYSIS

The data were analyzed in a Hund's case ( $b$ ) basis, as appropriate for these molecules, using  ${}^3\Sigma^-$  and  ${}^6\Sigma^+$  effective

TABLE IV. Spectroscopic constants for CrC ( $X^3\Sigma^-$ ).<sup>a</sup>

Parameter	Millimeter-wave	Optical <sup>b</sup>
B	19 480.742 4(92)	19 785(44)
D	0.049 168 2(24)	...
$\gamma$	-59.75(63)	-1 980(1 800)
$\gamma_D$	-0.000 91(87)	...
$\lambda$	178 011(11)	202 100(21 000)
$\lambda_D$	-1.496 7(48)	...
rms	0.067	...

<sup>a</sup>In MHz; values in parentheses are 3 $\sigma$  errors.<sup>b</sup>Reference 25.

Hamiltonians for CrC and CrCCH/CrCCD, respectively. These Hamiltonians consists of three major terms: rotation, spin-spin interactions, and spin-rotation coupling,

$$\mathbf{H}_{eff} = \mathbf{H}_{rot} + \mathbf{H}_{ss} + \mathbf{H}_{sr}. \quad (1)$$

The data were fit with the nonlinear least-squares analysis program HUND B to establish spectroscopic parameters. For the high spin  $^6\Sigma^+$  term, use of the fourth-order spin-spin parameter  $\theta$  slightly improved the fit, but use of third-order rotation constant  $\gamma_s$  did not. (For definitions of these parameters, see Ref. 29). Resulting constants are listed in Tables IV (CrC) and V (CrCCH).

As shown in Table IV, six parameters were required to accurately fit the data for CrC, including centrifugal distortion corrections  $\lambda_D$  and  $\gamma_D$ , resulting in an rms of 67 kHz. Also listed in the table are the constants derived by Brugh *et al.*<sup>25</sup> from their resonant two-photon ionization study of the  $^3\Sigma^- - X^3\Sigma^-$  electronic transition. Our rotational constant differs by about 300 MHz from that of Brugh *et al.*, and our spin-rotation parameter is significantly smaller. These authors fit the ground state with only three constants, B,  $\lambda$ , and  $\gamma$ , however, noting a high degree of correlation of the rotational and spin parameters between the ground and excited states. The differences between the mm-wave and optical values are likely a result of this correlation.

The resulting constants for CrCCH are in excellent agreement with the optical work of Brugh and Morse,<sup>26</sup> as displayed in Table V. There is some variation in the spin-spin constant  $\lambda$  due to the inclusion of  $\theta$  in our analysis; Brugh and Morse fixed this parameter to zero in their fit. If we do the same, then the derived spin-spin constant is within 0.5 MHz of that of Brugh and Morse. The constants for CrCCD scale

TABLE V. Spectroscopic constants for CrCCH and CrCCD ( $\bar{X}^6\Sigma^+$ ).<sup>a</sup>

Parameters	CrCCH	CrCCD	CrCCH: optical <sup>b</sup>
B	3 846.058 64(99)	3 537.056 5(42)	3845.71(90)
D	0.001 223 68(15)	0.000 976 71(49)	...
$\gamma$	48.683(31)	44.848(34)	46.9(2.2)
$\lambda$	8 714(11)	8 675(28)	8689.5(9.0)
$\lambda_D$	-0.003 42(13)	-0.002 975(91)	0.12(11)
$\theta$	-6.5(3.3)	...	...
rms	0.080	0.049	221

<sup>a</sup>In MHz; values in parentheses are 3 $\sigma$  errors.<sup>b</sup>Reference 26.

as expected for a slightly heavier molecule. The rms values of the fits are 80 kHz for CrCCH and 49 kHz for CrCCD, which are within the experimental accuracy.

## V. DISCUSSION

The pure rotational measurements of CrC have resulted in improved spectroscopic parameters for this free radical. From the refined rotational constant, the  $r_0$  bond length of this molecule was found to be 1.6314 Å. This distance is longer than the value derived by Brugh *et al.* of 1.6188 Å,<sup>25</sup> as expected, given the differences in B. The bond distance in CrC is comparable to that in NiC, which has  $r_0 = 1.6308$  Å<sup>16</sup>—both of which are larger than those in FeC (1.5931 Å) and CoC (1.5612 Å).<sup>15,16</sup>

CrC is thought to have an electron configuration of  $8\sigma^2 3\pi^4 1\delta^2$ , with the  $8\sigma$  and  $3\pi$  orbitals creating a triple bond.<sup>25</sup> NiC is also thought to have a triple bond and an  $8\sigma^2 9\sigma^2 3\pi^4 1\delta^4$  configuration, with the additional 4 electrons filling the non-bonding  $1\delta$  and  $9\sigma$  orbitals.<sup>16</sup> The  $9\sigma$  orbital in this case is primarily composed of the  $4s$  orbital of nickel. It is therefore not surprising that CrC and NiC have similar bond lengths. The decrease in bond distance for the iron and cobalt carbides at least partially reflects a corresponding decrease in atomic radii across the periodic table.

For CrCCH, more isotopic substitutions are needed to derive an accurate structure, which is work in progress. However, if the assumption is made that the acetylenic ligand in CrCCH is similar to that in ZnCCH and CuCCH, then the Cr—C bond distance can be estimated. This assumption is reasonable given that ZnCCH and CuCCH have comparable C—C and C—H bond distances. If  $r(\text{C—H}) = 1.048$  Å and  $r(\text{C}\equiv\text{C}) = 1.238$  Å is assumed for CrCCH, based on the zinc analog, then the Cr—C bond distance is found to be 1.993(6) Å, derived from the two measured rotational constants. This metal-carbon bond distance is longer than that in ZnCCH and CuCCH by 0.09 and 0.17 Å, respectively (see Table VI). This lengthening likely reflects the presence of 5 unpaired electrons on the metal nucleus, as opposed to one (ZnCCH) or zero (CuCCH), as well as the general trend in atomic radii. It is also significantly longer than in CrC by almost 0.4 Å, but similar to that in CrCN, which is 2.023 Å.<sup>29</sup> Both the acetylide and the cyanide appear to exhibit single chromium-carbon bonds, while that in the monocarbide is a triple bond. The bond lengths reflect this change in bond order.

According to Brugh *et al.*,<sup>25</sup> there is substantial amount of spin-orbit interactions between the  $^3\Sigma^-$  ground state of CrC, the subject of this study, and the closest isoconfigurational  $^1\Sigma^+$  excited state, which occurs through the one electron spin-orbit operator  $\sum_i a_i \mathbf{l}_i \cdot \mathbf{s}_i$ .<sup>31</sup> Here  $a_i$  is the spin-orbit constant of the  $i$ th electron. The  $^1\Sigma^+$  state is generated by pairing of the spins of the two  $\delta$  electrons. Other possible perturbing terms such as  $^1\Pi$ ,  $^3\Sigma^+$ , and  $^3\Pi$  are not predicted to be as close in energy.<sup>25</sup> The  $^3\Sigma^- - ^1\Sigma^+$  coupling can increase the spin-spin constant  $\lambda$  by providing a second-order contribution. As a consequence, the  $\Omega = 0$  levels of the ground state of CrC are perturbed relative to  $\Omega = \pm 1$  levels, as is observed in the energy levels of this molecule: see Figure 1. Considering the case (a) limit where

TABLE VI. Structures of CrCCH and related species.

Molecule	$r(\text{M}-\text{C})$ (Å)	$r(\text{C}-\text{C})$ (Å)	$r(\text{C}-\text{H})$ (Å)	Method	Reference
CrCCH ( $\tilde{X}^6\Sigma^+$ )	1.993(6)	1.238 <sup>a</sup>	1.048 <sup>a</sup>	$r_0$	This work
ZnCCH ( $\tilde{X}^2\Sigma^+$ )	1.902(3)	1.238(4)	1.048(1)	$r_0$	18
CuCCH ( $\tilde{X}^1\Sigma^+$ )	1.9083(3)	1.231 3(3)	1.0508(1)	$r_m^{(1)}$	17
	1.818(1)	1.212(2)	1.058(1)	$r_0$	
	1.822(1)	1.213(2)	1.058(1)	$r_m^{(1)}$	
	1.8177(6)	1.217 4(6)	1.046(2)	$r_m^{(2)}$	
HC≡CH	1.834	1.212	1.062	$r_e$ , B3LYP	
CrCN ( $\tilde{X}^6\Sigma^+$ )	2.0232(8)	1.202 41(9)	1.0625(1)	$r_e$ , IR, Raman	30
	2.019			$r_0$ $r_m^{(1)}$	29

<sup>a</sup>Value fixed.

$J$  and  $\Omega$  are the good quantum numbers, the  $\Omega = 0$  sub-level is pushed to lower energy than the corresponding  $\Omega = \pm 1$  levels for a given  $J$ . The figure illustrates this effect for the  $J = 11$  levels, shown in bold.

If it is assumed that the main contribution to the spin-spin constant is second order spin-rotation coupling (i.e.,  $\lambda \sim \lambda^{SO}$ ), and that the main perturber is the nearest  $^1\Sigma^+$  term, then energy of this state can be estimated from the equation<sup>31</sup>

$$\lambda^{SO} = \frac{-30(2S-2)!}{(2S+3)!} \times \sum_{\Sigma} \sum_{n', \Lambda', S', \Sigma'} \frac{[3\Sigma^2 - S(S+1)] |\langle n', \Lambda', S', \Sigma' | \hat{H}_{SO} | n, \Lambda, S, \Sigma \rangle|^2}{E_{n'} - E_n}. \quad (2)$$

The quantum numbers  $n'$ ,  $\Lambda'$ ,  $S'$ , and  $\Sigma'$  sum over nearby perturbing states, in this case the  $^1\Sigma$  state. The one-electron spin-orbit operator,  $\mathbf{H}_{SO} = \sum_i a_i \mathbf{l}_i s_i$ , follows the selection rules  $\Delta S = 0, \pm 1$ ,  $\Delta \Omega = 0$ ,  $\Delta \Sigma = -\Delta \Lambda = 0, \mp 1$ , and  $\Sigma^\pm \leftrightarrow \Sigma^\mp$ . Considering the  $^1\Sigma$  state only, Equation (2) simplifies to

$$\lambda^{SO} = \frac{-30(2S-2)!}{(2S+3)!} \times \frac{[3\Sigma^2 - S(S+1)] |\langle a^1\Sigma_0 | \sum a_i \mathbf{l}_i s_i | X^3\Sigma_0 \rangle|^2}{E(^1\Sigma^+) - E(X^3\Sigma^-)}. \quad (3)$$

The Slater determinants for the two connecting states are

$$\begin{aligned} |X^3\Sigma_0^- \rangle &= \frac{1}{\sqrt{2}} [\delta^+ \alpha \delta^- \beta + \delta^+ \beta \delta^- \alpha], \\ |^1\Sigma_0^+ \rangle &= \frac{1}{\sqrt{2}} [\delta^+ \alpha \delta^- \beta - \delta^+ \beta \delta^- \alpha]. \end{aligned} \quad (4)$$

Equation (3) then further simplifies to the expression

$$\lambda^{SO} \sim 2a^2 / \Delta E(^1\Sigma^+ - ^3\Sigma^-). \quad (5)$$

Here  $a$  is assumed to be that of  $\text{Cr}^+$  ( $a = 224 \text{ cm}^{-1}$ ), and  $\Delta E(^1\Sigma^+ - ^3\Sigma^-)$  is the energy difference between the ground and  $^1\Sigma^+$  excited state. Assuming  $\lambda^{SO} \sim 178\,011 \text{ MHz} = 5.94 \text{ cm}^{-1}$ , then the isoconfigurational  $^1\Sigma^+$  state lies  $\sim 16\,900 \text{ cm}^{-1}$  above the ground state. This value is not unreasonable, considering that closest three excited triplet states in CrC are calculated

theoretically to lie  $\sim 2800$ – $11\,800 \text{ cm}^{-1}$  above the ground state.<sup>25</sup>

For CrCCH, the value of  $\lambda$  (8714 MHz) is about the same magnitude as in other chromium containing molecules with  $^6\Sigma^+$  ground states, including CrH (6980 MHz)<sup>32</sup> and CrCl (7989 MHz).<sup>33</sup> One glaring exception is CrCN, which has a much smaller value of  $\lambda = 640 \text{ MHz}$ . These differences can be understood in terms of Equation (2). Because of selection rules (see above), the spin-orbit operator can connect the ground state in CrCCH to a range of excited states, and the most important are  $^4\Sigma^-$ ,  $^4\Pi$ , and  $^6\Pi$ . Octet and  $^6\Sigma^-$  states are also possible, but as discussed by Flory *et al.*,<sup>29</sup> these require excitation of core electrons and thus lie very high in energy. There are four  $^4\Sigma^-$ , eight  $^4\Pi$ , and one  $^6\Pi$  states to consider. The matrix elements involving the excited  $^4\Sigma^-$  and  $^6\Pi$  states yield a positive contribution to  $\lambda$ , while the  $^4\Pi$  terms give a negative one. For CrCN, the overall effect significantly reduces the value of  $\lambda$ , but such a reduction is not nearly as drastic in CrCCH, CrH, and CrCl. This result suggests that the electronic state manifolds of the monoacetylide, hydride, and chloride are comparable and differ from that of the cyanide.

In analogy to CrCN, only the excited  $^6\Pi$  state can contribute to  $\gamma$  because the operator  $\hat{H}_{rot} = \mathbf{BL}_\pm$  requires the selection rule  $\Delta S = 0$ . Assuming that the major contribution to  $\gamma$  is second-order spin-orbit coupling, the energy of the nearby  $^6\Pi$  state can be estimated from the formula given by Lefebvre-Brion and Field,<sup>34</sup>

$$\gamma^{SO} = 2 \left[ \langle ^6\Pi_{5/2} | B(r) \mathbf{L}_+ | ^6\Sigma_{3/2}^+ \rangle \langle ^6\Sigma_{5/2}^+ | H_{SO} | ^6\Pi_{5/2} \rangle + \langle ^6\Pi_{3/2} | H_{SO} | ^6\Sigma_{3/2}^+ \rangle \langle ^6\Sigma_{5/2}^+ | B(r) \mathbf{L}_- | ^6\Pi_{3/2} \rangle \right] / \Delta E_{\Pi\Sigma} \langle ^6\Sigma_{5/2}^+ | \mathbf{J} \cdot \mathbf{S} | ^6\Sigma_{3/2}^+ \rangle. \quad (6)$$

As discussed in Ref. 29, to evaluate this equation, the operator  $L_{\pm}$  must be reduced to the form  $\sum I_{i\pm}$  and operate on the chromium atomic wave function  $\Psi = \frac{1}{\sqrt{2}} [|s\sigma\rangle \pm |d\sigma\rangle]$ —not very good approximations. Nevertheless, with the additional assumption that  $B(r) \sim B(\bar{X}^6\Sigma^+)$ , Equation (6) can be reduced to the simple expression

$$\gamma^{SO} = \frac{0.271 \cdot B \cdot a}{\Delta E(^6\Pi-^6\Sigma^+)}. \quad (7)$$

Using the experimentally determined values of  $B = 0.12829 \text{ cm}^{-1}$  and  $\gamma = 0.00162 \text{ cm}^{-1}$ , and the atomic  $\text{Cr}^+$   $a$  value, the energy of the excited  $^6\Pi$  state is estimated to be  $\Delta E(^6\Pi-^6\Sigma^+) \sim 4800 \text{ cm}^{-1}$ —about a factor of two less than the experimentally determined values for  $\text{CrCl}$  and  $\text{CrF}$  of  $\Delta E(^6\Pi-^6\Sigma^+) \sim 8850 \text{ cm}^{-1}$  and  $\Delta E(^6\Pi-^6\Sigma^+) \sim 8134 \text{ cm}^{-1}$ , respectively.<sup>35</sup> This energy is also lower than that of the  $A^6\Sigma^+$  state, as measured experimentally.<sup>26</sup>

## VI. CONCLUSION

Evaluating the fundamental properties of small, Cr-containing molecules aids in understanding the role of chromium in more complex chemical systems. This study of the pure rotational spectra of  $\text{CrC}$  and  $\text{CrCCH}$  demonstrates that the ground states of these two radicals are  $^3\Sigma^-$  and  $^6\Sigma^+$ , respectively, verifying previous optical work. In  $\text{CrC}$ , chromium appears to form a triple bond with the carbon atom, while a single bond is formed in  $\text{CrCCH}$ . The single bond in the latter species suggest that the  $-\text{CCH}$  ligand retains its basic acetylenic structure, as has been found in  $\text{ZnCCH}$  and  $\text{CuCCH}$ . Spectroscopic studies of other chromium-bearing molecules would give additional insight into transition metal bonding.

## ACKNOWLEDGMENTS

This research was supported by NSF Grant Nos. AST-1211502, AST-1515568, and CHE-1057924.

<sup>1</sup>K. H. Theopold and R. R. Kucharczyk, *Chromium: Organometallic Chemistry. Encyclopedia of Inorganic Chemistry* (John Wiley and Sons, New York, 2006).

<sup>2</sup>E. O. Fischer and W. Hafner, *Z. Naturforsch. B* **8**, 444–445 (1953).

<sup>3</sup>Y. Meng, Y. Han, H. Zhu, Z. Yang, K. Shen, B. Suo, Y. Lei, G. Zhai, and Z. Wen, *Int. J. Hydrogen Energy* **40**, 12047–12056 (2015).

<sup>4</sup>J. S. Pilgrim and M. A. Duncan, *J. Am. Chem. Soc.* **115**, 6958–6961 (1993).

<sup>5</sup>A. A. Popov, S. Yang, and L. Dunsch, *Chem. Rev.* **113**, 5989–6113 (2013).

<sup>6</sup>O. Loboda, *Quantum-Chemical Studies on Porphyrins, Fullerenes, and Carbon Nanostructures* (Springer-Verlag, Berlin, 2013).

<sup>7</sup>L. Qian, L. Norin, J. H. Guo, C. Sathe, A. Agui, U. Jansson, and J. Nordgren, *Phys. Rev. B* **59**, 12667–12671 (1999).

<sup>8</sup>V. M. Rayón, P. Redondo, C. Barrientos, and A. Largo, *Chem. Eur. J.* **12**, 6963–6975 (2006).

<sup>9</sup>J. Min, D. T. Halfen, and L. M. Ziurys, *Chem. Phys. Lett.* **609**, 70–75 (2014).

<sup>10</sup>Y. C. Chang, C. S. Lam, B. Reed, K. C. Lau, H. Liou, and C. Ng, *J. Phys. Chem. A* **113**, 4242–4248 (2009).

<sup>11</sup>H. Huang, Y. C. Chang, Z. Luo, X. Shi, C.-S. Lam, K. C. Lau, and C. Ng, *J. Chem. Phys.* **138**, 094301/1–094301/9 (2013).

<sup>12</sup>Y. C. Chang, X. Shi, K. C. Lau, Q. Z. Yin, H. T. Liou, and C. Ng, *J. Chem. Phys.* **133**, 054310/1–054310/10 (2010).

<sup>13</sup>O. Krechkivska and M. D. Morse, *J. Phys. Chem. A* **117**, 13284–13291 (2013).

<sup>14</sup>Z. Luo, H. Huang, Y. C. Chang, Z. Zhang, Q. Yin, and C. Y. Ng, *J. Chem. Phys.* **141**, 144307 (2014).

<sup>15</sup>P. M. Sheridan, L. M. Ziurys, and T. Hirano, *Astrophys. J., Lett.* **593**, 141–144 (2003).

<sup>16</sup>M. A. Brewster and L. M. Ziurys, *Astrophys. J.* **559**, 163–166 (2001).

<sup>17</sup>M. Sun, D. T. Halfen, J. Min, B. Harris, D. J. Clouthier, and L. M. Ziurys, *J. Chem. Phys.* **133**, 174301/1–174301/8 (2010).

<sup>18</sup>J. Min, D. T. Halfen, M. Sun, B. Harris, and L. M. Ziurys, *J. Chem. Phys.* **136**, 244310/1–244310/10 (2012).

<sup>19</sup>E. L. Johnson and M. D. Morse, *Mol. Phys.* **113**, 2255–2266 (2015).

<sup>20</sup>M. A. Garcia and M. D. Morse, *J. Phys. Chem. A* **117**, 9860–9870 (2013).

<sup>21</sup>M. Barnes, P. G. Hajigeorgiou, R. Kasrai, A. J. Merer, and G. F. Metha, *J. Am. Chem. Soc.* **117**, 2096–2097 (1995).

<sup>22</sup>M. Barnes, A. J. Merer, and G. F. Metha, *J. Mol. Spectrosc.* **181**, 168–179 (1997).

<sup>23</sup>D. B. Grotjahn, D. T. Halfen, L. M. Ziurys, and A. L. Cooks, *J. Am. Chem. Soc.* **126**, 12621–12627 (2004).

<sup>24</sup>D. J. Brugh, R. S. DaBell, and M. D. Morse, *J. Chem. Phys.* **121**, 12379/1–12379/7 (2004).

<sup>25</sup>D. J. Brugh, M. D. Morse, A. Kalemios, and A. Mavridis, *J. Chem. Phys.* **133**, 034303/1–034303/8 (2010).

<sup>26</sup>D. J. Brugh and M. D. Morse, *J. Chem. Phys.* **141**, 064304/1–064304/9 (2014).

<sup>27</sup>C. Savage and L. M. Ziurys, *Rev. Sci. Instrum.* **76**, 043106/1–043106/6 (2005).

<sup>28</sup>D. T. Halfen and L. M. Ziurys, *J. Mol. Spectrosc.* **234**, 34–40 (2005).

<sup>29</sup>M. A. Flory, R. W. Field, and L. M. Ziurys, *Mol. Phys.* **105**, 585–597 (2007).

<sup>30</sup>E. Kostyk and H. L. Welsh, *Can. J. Phys.* **58**, 534–543 (1980).

<sup>31</sup>J. M. Brown, E. A. Colbourn, J. K. G. Watson, and F. D. Wayne, *J. Mol. Spectrosc.* **74**, 294–318 (1979).

<sup>32</sup>D. T. Halfen and L. M. Ziurys, *Astrophys. J.* **611**, L65–68 (2004).

<sup>33</sup>K. Katoh, T. Okabayashi, M. Tanimoto, Y. Sumiyoshi, and Y. Endo, *J. Chem. Phys.* **120**, 7927/1–7927/6 (2004).

<sup>34</sup>H. Lefebvre-Brion and R. W. Field, *The Spectra and Dynamics of Diatomic Molecules* (Elsevier, New York, 2004).

<sup>35</sup>J. F. Harrison and J. H. Hutchison, *Mol. Phys.* **97**, 1009–1027 (1999).